A 6-yr Cloud-to-Ground Lightning Climatology and Its Relationship to Rainfall over Central and Eastern China

RUDI XIA

State Key Laboratory of Severe Weather, Chinese Academy of Meteorological Sciences, Beijing, China

DA-LIN ZHANG

State Key Laboratory of Severe Weather, Chinese Academy of Meteorological Sciences, Beijing, China, and Department of Atmospheric and Oceanic Science, University of Maryland, College Park, College Park, Maryland

BAILIN WANG

Meteorological Observation Center, China Meteorological Administration, Beijing, China

(Manuscript received 15 January 2015, in final form 14 August 2015)

ABSTRACT

The cloud-to-ground (CG) lightning climatology and its relationship to rainfall over central and eastern China is examined, using data from 32 million CG lightning flashes and Tropical Rainfall Measuring Mission measurements during a 6-yr period covering 2008–13. Results show substantial spatial and temporal variations of flash density across China. Flash counts are the highest (lowest) in summer (winter) with the lowest (highest) proportion of positive flashes. CG lightning over northern China is more active only in summer, whereas in winter CG lightning is more active only in the Yangtze River basin. The highest CG lightning densities, exceeding 9 flashes per kilometer squared per year and more than 70 CG lightning days per year, are found in the northern Pearl River delta region, followed by the Sichuan basin, the Yangtze River delta, and the southeastern coast of China in that order. Lower-flash-density days occur over mountainous regions as a result of the development of short-lived afternoon storms, while higher-flash-density days, typically associated with nocturnal thunderstorms, appear over the north China plain and Sichuan basin. The highest number of CG lightning flashes is found in August whereas monthly convective rainfall peaks in May or July. Flash rates during the warm season are typically maximized in the afternoon hours in coincidence with a convective rainfall peak except for the Sichuan basin and its surrounding mountainous areas where a single late-night convective rainfall peak dominates. Much less lightning activity corresponds to a late-night to morning rainfall peak over the plains in eastern China because of the increased proportion of stratiform rainfall during that period.

1. Introduction

Cloud-to-ground (CG) lightning, accounting for about 25% of total lightning including both CG and intracloud lightning, is one of the major causes of weather-related fatalities in China. According to Zhang et al. (2011), CG lightning caused 5022 deaths and 4670 injuries during the years 1997–2009. The annual fatality rate per million people in China is between 0.31 (Zhang et al. 2011) and 0.53 (Ma et al. 2008), which is close to the 0.42 rate found in the United States (Curran et al. 2000). Considering China's large population and its higher population density over its coastal regions, the number of lightning-related casualties in China should be greater than that in the United States. Thus, it is highly desirable to investigate the CG lightning climatology across China for the purpose of severe weather warning and disaster prevention.

CG lightning climatological studies began in the 1960s for the continental United States, and bloomed since the setup of the U.S. National Lightning Detection Network (NLDN; Orville 2008) in the late 1980s. The earliest study of Changnon (1964) examined the distribution and monthly variation of CG lightning in Illinois during 1914–47 using limited records from the U.S. Weather Bureau. In the late 1980s, CG lightning climatology,

Corresponding author address: Dr. Rudi Xia, State Key Laboratory of Severe Weather, Chinese Academy of Meteorological Sciences, Beijing 100081, China.
E-mail: xiarudi@gmail.com

DOI: 10.1175/JAMC-D-15-0029.1

© 2015 American Meteorological Society

based on a few sensors that collected data over a couple of years, added some new knowledge of diurnal variations of CG lightning in some parts of the United States (López and Holle 1986; Reap and MacGorman 1989). Subsequently, numerous CG lightning climatological studies using 6–16 yr of data have been published (Watson et al. 1994; Livingston et al. 1996; Huffines and Orville 1999; Bentley and Stallins 2005; Vogt and Hodanish 2014; Chronis et al. 2015; Koshak et al. 2015). Results show pronounced variability in the spatial and temporal (from annual to diurnal) distributions of CG lightning. The multiplicity of CG lightning, the proportion of positive versus negative CG lightning, and the magnitude of first-stroke peak currents have also been documented in some of those studies. Numerous studies of CG lightning climatology have also been conducted over the other areas in the Northern Hemisphere since the late 1990s (e.g., Hidayat and Ishii 1998; Rivas Soriano et al. 2005; Antonescu and Burcea 2010; Enno 2011; Novák and Kyznarová 2011).

The previous studies show that the general shape and central location, as well as the annual and diurnal cycles of CG lightning over the continental United States, remain almost the same in spite of different time spans of the data used. The maximum annual CG lightning flash density was found in Florida, with 9–11 flashes per kilometer squared per year (hereinafter flashes $km^{-2} yr^{-1}$) on a 0.2°-resolution grid (Huffines and Orville 1999; Orville and Huffines 2001), although occasionally this maximum was located in the Midwest with 11–13 flashes $km^{-2} yr^{-1}$ (Orville and Silver 1997). These studies all showed the highest and lowest CG lightning flash counts occurring in summer and winter, respectively. However, there were regional differences in the CG lightning diurnal cycle because of the different impacts of solar heating, topography, and underlying surface conditions. Most land areas had peaks in the afternoon hours except for the areas surrounded by high mountains where CG lightning peaked at night. Over water, CG lightning peaked at night or in the early morning hours. For example, the afternoon CG lightning peak during the warm season had been found by Watson et al. (1994) for Arizona, Rivas Soriano et al. (2005) for the Iberian Peninsula, Enno (2011) over land in Estonia, Novák and Kyznarová (2011) for the Czech Republic, and Hidayat and Ishii (1998) for the island of Java. The peak CG lightning hours over seas in Estonia were 1300–2100 local standard time (LST; Enno 2011), whereas the peak CG lightning over water surrounding the continental United States occurred during 0400–1200 LST (Orville and Huffines 2001). Additionally, a late evening peak between 2000 and 0400 LST was observed for the upper Midwest. The proportion of positive CG lightning documented by those studies was the lowest to several percentiles in summer and the highest up to around 25% in winter [see Orville and Huffines (2001) for the United States; Bentley and Stallins (2005) for Georgia; Rivas Soriano et al. (2005) for the Iberian Peninsula; Antonescu and Burcea (2010) for Romania]. The CG lightning density is sometimes greater over sloping terrain (Fosdick and Watson 1995; López et al. 1997; Antonescu and Burcea 2010).

Climatological studies of CG lightning in China did not start until the late 2000s when its National Lightning Detection Network began to be set up and expanded. But most of the studies focused on CG lightning characteristics over a few areas because of the lack of long-term data coverage. Nevertheless, as soon as a regional lighting network was established, the China Meteorological Administration (CMA) began to digitize CG lightning strokes on a daily basis, and now includes the spatial distribution, monthly CG lightning counts, and the number of CG lightning days over 26 provinces/districts, as well as CG lightning strokes over many airports, ports, and power plants (CMA 2009, 2010, 2011, 2013) that cover almost all of central and eastern China (see Fig. 1 for their coverage). The annual operation rates of lightning sensors have also been recorded.

While the spatial and temporal variations of CG lightning over most of continental China have been recorded, few CG lightning climatological studies, like those obtained in the United States and elsewhere, were conducted using the recorded data. Little, however, is known about the diurnal to annual cycles of CG lightning and their spatial variations across China. Thus, it is the intention of this study to fill in this gap. Both the satellite observations and the reports of economic losses attributable to natural disasters indicated that the lightning density and lightning-related losses in western China were much smaller than those in central and eastern China (Ma et al. 2008; Zhang et al. 2011), despite the presence of a high number of thunder days over the Tibetan Plateau. In addition, the CG lightning detection network had not been expanded to cover all of western China. Thus, we could focus mainly on characterizing the spatial and temporal (i.e., from diurnal to annual) variations of CG lightning over central and eastern China using a 6-yr (2008–13) dataset.

The next section describes the data source and methodology used for the present study. Section 3 shows the CG lightning climatology with regional variations over central and eastern China. Previous studies for the associated CG-lightning-producing weather systems will also be discussed. Section 4 presents a (convective and stratiform) precipitation climatology and its monthly to diurnal variations in relation to the corresponding CG lightning climatology. A summary and concluding remarks are given in the final section.

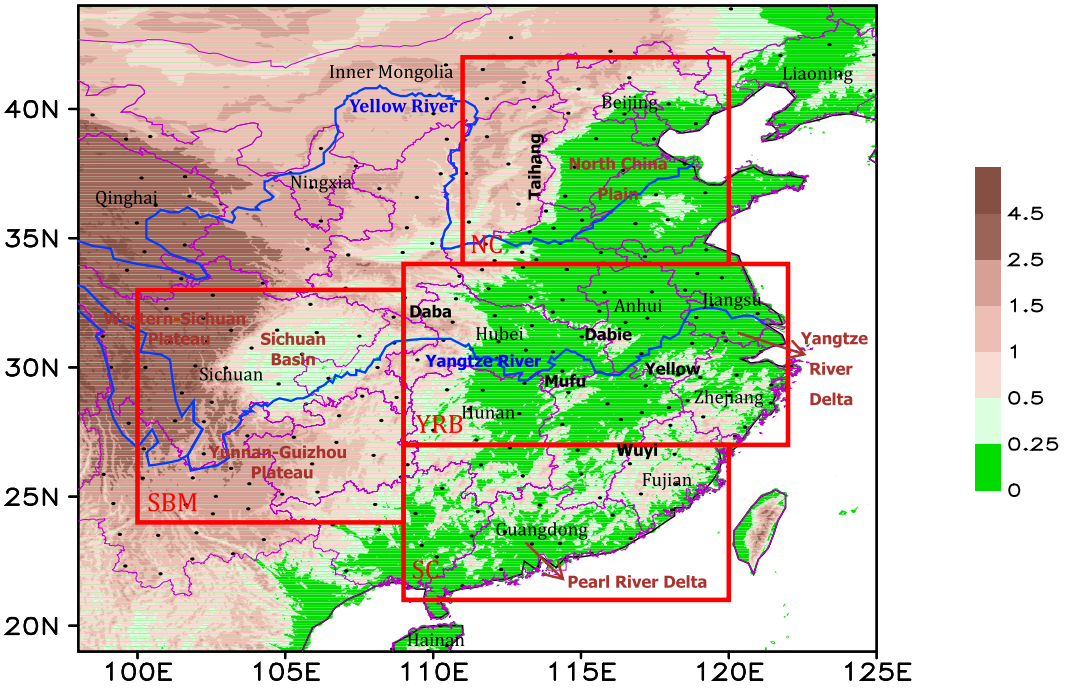

FIG. 1. Distribution of topography (shaded; km) and ADTD lightning sensors (black dots) over most of continental China. Blue curved lines represent major rivers, and purple curved lines denote provincial borders. Provincial names and major mountains are shown in thin and boldface black fonts, respectively. Rectangles in red denote the target regions of NC (34°–42°N, 111°–120°E), YRB (27°–34°N, 109°–122°E), SBM (24°–33°N, 100°–109°E), and SC (21°–27°N, 109°–120°E), as is the case for the remaining figures.

2. Data source and method

The National Lightning Detection Network in China, shown in Fig. 1, has been installed with ground-based Advanced Time of Arrival and Direction (ADTD) system CG lightning detection sensors, the number of which increased from 183 with an average operation rate of 88.97% in 2008 to 357 with an average operation rate of greater than 95% in 2013 (CMA 2009). The operational network provides reports on the time of the returning stroke, and its location (latitude and longitude), polarity, and peak current. In 2008, many parts of Inner Mongolia; Ningxia, Liaoning, and Jilin Provinces/Districts (in northern China); and of Anhui (in east China), Hainan, and the northern Guangdong Provinces (in southern China) remained void of CG lightning detection sensors (CMA 2009). This CG lightning detection coverage was improved at the end of 2009 after installing 80 additional sensors (CMA 2010). As a result, the ADTD CG lightning detection sensors have since covered almost all parts of central and eastern China (Fig. 1).

In this study, some data quality control has been performed by removing positive ground strokes of less than 15 kA, following Cummins and Murphy (2009), in order to eliminate possible cloud discharge contaminations. In addition, only the first stroke's data are retained by applying the stroke-grouping algorithm developed by Cummins et al. (1998), which may consist of a series of separate strokes that occurred for 1-s time periods within 10 km of the first stroke detected, with the time interval from the previous stroke of less than 0.5 s.

Given the distribution of CG lightning detection sensors in Fig. 1, we select the following four "target regions" for the present study: (i) northern China (NC), (ii) the middle and lower reaches of the Yangtze River basin (YRB), (iii) southern China (SC), and (iv) the Sichuan basin and its surrounding mountainous areas (SBM). On the geographic map the first three regions may be considered to be part of eastern China, and SBM as part of central China. These four regions are selected because they have distinct characteristics in local topography and climatological regime. For example, most of eastern and southern China are basically plain areas with low-elevation mountains or hills, whereas SBM is distributed with high and complex topography around a basin. In contrast, NC includes Mount Taihang of 1500–2500 m in elevation to the west, which is southwest–northeast oriented, and plain areas to the southeast. Climatologically, NC is nearly a semiarid region, especially in its northwest portion, whereas the other three regions are

dominated by the East Asian monsoon with ample rainfall during the growing season (Ding and Chan 2005). The warm and moist monsoon air can also extend into the northern plain areas. As will be seen in the next two sections, these topographical and climatological differences have important implications for the regional CG lightning (and rainfall) climatology.

As Fig. 1 shows, more than half of the 357 CG lightning sensors are relatively uniformly distributed in the four target regions, giving roughly a horizontal resolution of less than 1.5° latitude/longitude. As estimated by its manufacturer, the ADTD CG lightning detection network in central and eastern China has a detection efficiency of 90% and a location accuracy of about 500 m within a radius of 150 km. [We should mention that the location accuracy and detection efficiency of this network had not been systematically evaluated because of the lack of adequate ground truths. However, according to Prof. Y. Zhang (2014, personal communication), the location errors of the Chinese NLDN over Guangdong Province were about 2 km, using the ground truth from artificially triggered lightning experiments.] The CG lightning reports are objectively analyzed on a grid with 0.2° horizontal resolution and roughly 20-km cells. As mentioned by Huffines and Orville (1999) and Orville and Silver (1997), with the 20-km horizontal resolution, location errors on the order of 10 km would affect little the climatological distribution of CG lightning. Moreover, if the detection efficiency has few regional differences, it may underestimate the quantitative analyses of the multiplicity of flashes and flash-density values, but affect little the qualitative analyses of the monthly and diurnal variation tendencies of flashes within the valid perimeter of lightning detection sensors.

Horizontal resolution of about 20 km has been widely used to obtain annual CG lightning flash-density maps, and it seems to be quite appropriate for large-scale climatological studies (Watson et al. 1994; Huffines and Orville 1999; Orville and Huffines 2001; Rivas Soriano et al. 2005). Higher horizontal resolution data have been used for some special studies. For example, 2.6-km-resolution CG lightning data have been used for risk assessment for the 1996 Summer Olympics in Georgia (Livingston et al. 1996), and 10-m resolution data have been used to analyze the roles of local topography in inducing CG lightning activity (Vogt and Hodanish 2014). Clearly, horizontal resolution should have little impact on the CG lightning pattern but will likely have more of an influence on the magnitude of maximum and minimum values when denser-resolution data are used. Novák and Kyznarová (2011) showed that the maximum value in the Czech Republic is 3.23 flashes $km^{-2} yr^{-1}$ on 20 km × 20 km grids, and it doubles to

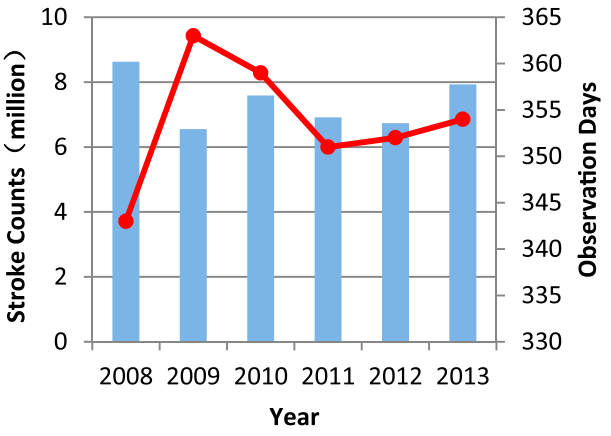

FIG. 2. Annual CG lightning stroke counts (blue bars, in millions) and the number of observation days (red) over the four target regions during 2008–13.

7.43 flashes $km^{-2} yr^{-1}$ on 1 km × 1 km grids for the period of 2002–08. One factor that may affect the CG lightning pattern is the correction of detection efficiency in regions outside the perimeter of the sensors. Murphy and Holle (2005) showed that northwestern Mexico became the densest CG lightning occurrence region in North America, instead of Florida, after correcting the detection efficiency in regions outside the perimeter of the sensors belonging to the U.S. National Lightning Detection Network.

Figure 2 shows that since its inception the CG lightning detection network has been on average collecting data for more than 350 days a year , with the exception of the first year of operation (i.e., 2008). This exception does not impose any problem for our study because a majority of missing days in 2008 are in December when thunderstorms were scarce. The CG lightning strokes are the lowest (i.e., ~6.55 millions) in 2009 although the number of sampling days in that year is the highest (i.e., 363 days). More than 32 million CG lightning flashes are observed across the four target regions during the 6-yr period of 2008–13 (see Table 1).

The Tropical Rainfall Measuring Mission (TRMM) Precipitation Radar (PR) 2A25, version 7, data products are used to distinguish convective from stratiform rainfall, in order to better link the lightning activity to precipitation. This dataset was acquired as part of NASA's Earth–Sun System Division, and it was archived and distributed by the Goddard Earth Sciences Data and Information Services Center Distributed Active Archive Center. In addition, the hourly precipitation data of 0.1° resolution during 2008–13 are used herein to provide the spatial distribution of rainfall over central and eastern China. This dataset was derived by merging rain gauge–based analyses and Climate Prediction Center morphing technique (CMORPH) satellite estimates through collaborations between the

TABLE 1. CG lightning summary for the four target regions during the 6-yr period of 2008–13.

Type	Positive	Negative	Total
No. of strokes	1 698 822	42 571 831	44 270 653
Total strokes (%)	3.84	96.16	—
No. of flashes	1 618 338	30 831 098	32 449 436
Total flashes (%)	4.99	95.01	—
Multiplicity	1.05	1.38	1.36

CMA's National Meteorological Information Center and the Climate Prediction Center (Xie and Xiong 2011; Pan et al. 2012).

3. Results

In this section, we discuss the statistical characteristics of the total CG lightning observations obtained across the four target regions and, then, analyze the spatial and temporal (i.e., from annual to monthly and diurnal) variations of CG lightning.

a. Statistical CG lightning characteristics in polarity, peak current, and multiplicity

Table 1 shows the statistical characteristics of CG lightning in terms of polarity and multiplicity. The 47 million CG lightning flashes detected during 2008–13 produce about 57 million strokes, of which about 77% occur in the four target regions over central and eastern China. We see that negative flashes account for 95% of the total flashes. The percentage of single-stroke lightning in the total CG lightning counts is about 77%, indicating that a majority of the CG lightning flashes produce single stokes. On average, most of the positive flashes have a multiplicity of 1.05, which is slight smaller than the monthly mean value of 1.2 for the U.S. NLDN. Negative flashes have a multiplicity of 1.38, which is smaller than the monthly mean value ranging from 2.1 to 2.5 for the U.S. NLDN (Orville and Huffines 2001). The lower multiplicity may reflect the relatively lower CG lightning stoke detection efficiency of the Chinese NLDN. However, the lower-efficiency issue should to a certain extent have less influence over our statistical analyses of lightning characteristics because lightning flash data are used herein.

The box-and-whisker plots of peak currents of the first strokes, which always take the greatest peak current among all of the strokes produced by any flash (Rakov and Uman 1990), are given in Fig. 3, showing that the 10th percentile of the first strokes' peak current of positive and negative flashes is close in magnitude with a small gap of 3.17 kA after excluding the positive CG lightning strokes with peak current of less than 15 kA. But the peak current gap between the two types of

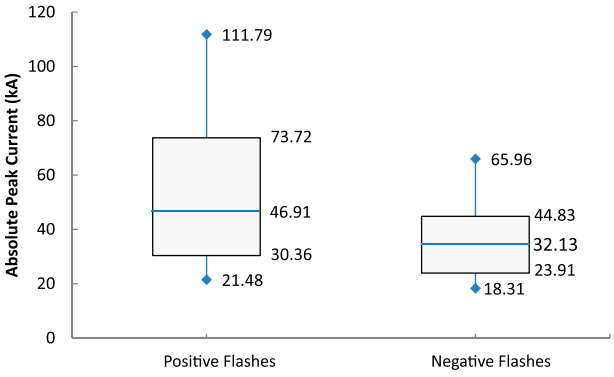

FIG. 3. Box-and-whisker plots of the averaged first-stroke peak current for the 6-yr period of 2008–13 over the four target regions. Boxes show interquartile ranges, whiskers show 10th and 90th percentile, and blue horizontal lines indicate the median value.

flashes increases gradually from 6.45 kA at the 25th percentile to 28.89 kA at the 75th percentile, indicating that positive flashes are better than negative flashes at producing large peak current strokes. The median first-stroke peak current is 46.91 kA for positive CG lightning flashes (excluding the peak current of less than 15 kA) and 32.13 kA for negative CG lightning flashes; both are greater than the decadal averages of 16.5 and 19.8 kA for the North American Lightning Detection Network, respectively (Orville et al. 2002). This may also indicate the relatively poorer detection sensitivity of the Chinese NLDN, since the median first-stroke peak current of the U.S. NLDN is about 10 kA for negative flashes and 32 kA for positive flashes from 1989 to 1998 with a range of 20–25 kA over 2000–10 (Chronis et al. 2015).

b. Spatial distribution of annual CG lightning flash density

Figure 4a shows that the annual CG lightning flash density varies greatly from less than 3 flashes $km^{-2} yr^{-1}$ in NC to more than 9 flashes $km^{-2} yr^{-1}$ in SC, which might be associated with different synoptic environments. Three distinct areas of high flash density can be seen: in the Yangtze River delta region, across central and south China, with a large "low-flash-density hole" in the middle. The most frequent CG lightning activity is found in the northern Pearl River delta region, with an annual density of 10.15 flashes $km^{-2} yr^{-1}$ in Zengcheng (23.2°N, 113.8°E) averaged for 2010–13 and 17.70 flashes $km^{-2} yr^{-1}$ in Huizhou (23.2°N, 114.6°E) averaged for 2008–09. Since CG lightning detection sensors did not completely cover Guangdong Province until 2010, the former peak flash-density location appears to be more credible. The coverage of the flash density exceeding 4 flashes $km^{-2} yr^{-1}$ extends westward to the western Guangdong region, where it is surrounded by complex

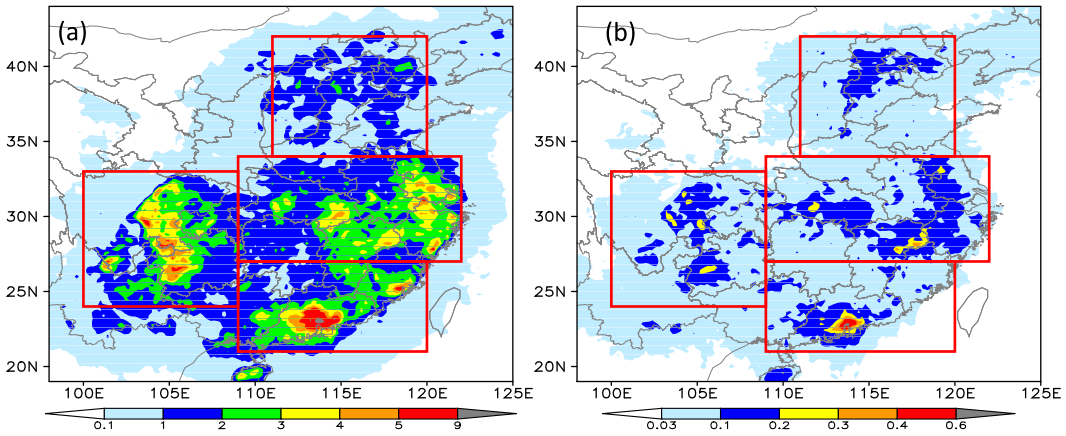

FIG. 4. Spatial distribution of the annual (a) CG lightning density and (b) positive CG lightning density (shaded, flashes $km^{-2}\,yr^{-1}$) at 0.2° × 0.2° grid resolution for the 6-yr period of 2008–13 over central and eastern China. CG lightning density over coastal oceans is masked with a small constant because of lacking observations, as is the case for the remaining figures.

terrain of less than 1500-m elevation. However, the flash density decreases sharply to the northwestward to less than 1 flash $km^{-2}\,yr^{-1}$ in Hunan Province. Another high-flash-density region is located in the northeast of SC, that is, over the southeastern coastal mountains of Fujian Province, which, together with its northeast–southwest-oriented flash band, results mostly from the interaction of the coastal mountains and sea breezes, plus some contributions from the passages of tropical cyclones.

The flash densities in northeast China and the surrounding areas of the four target regions are small, with typical values of less than 1 flash $km^{-2}\,yr^{-1}$, except for Hainan Province in south China. Most of the flashes in northeast China are likely generated in thunderstorms associated with extratropical cyclones and cold cutoff lows that occur all year round, and sometimes tropical storms or their interaction with extratropical cyclones (Wang et al. 2007). Nevertheless, the CG lightning climatology over this region is not of concern herein.

Shifting southwestward to lower latitudes, we see pronounced increases in flash density in the NC region, with several spots of 2–3 flashes $km^{-2}\,yr^{-1}$ located in the plains areas to the east of Mount Taihang. However, the CG lightning activity in this region is much weaker than in the other three target regions, which is consistent with the rainfall climatology shown in section 4. Previous studies showed the importance of topographical forcing and solar heating in generating afternoon thunderstorms that moved downstream to the eastern plain areas (He and Zhang 2010; Zhang et al. 2013). This region also frequently experiences the passage of cold frontal systems from the west, as well as east-to-northeastward intrusions of terrain-induced mesoscale cyclonic vortices from Qinghai Province (i.e., the so-called northwest vortex in China) and Sichuan Province (i.e., the so-called southwest vortex in China) during the months of July and August, respectively (Tao 1980). The two provinces are located on the respective north-to-northeast and eastern sides of the Tibet Plateau. The development of these different weather systems helps explain why NC's flash-density patterns are distinct from the surrounding regions.

The SBM region in central China exhibits several major flash centers, exceeding 4 flashes $km^{-2}\,yr^{-1}$ in the southwestern portion of the Sichuan basin and one center on the Yunnan–Guizhou Plateau. One can see strikingly steep gradients in flash density at the western edge of the basin where steep topography is present (cf. Figs. 4a and 1). These results agree well with those in the previous studies (e.g., Antonescu and Burcea 2010; Fosdick and Watson 1995; López et al. 1997) showing that the flash density is greater over sharp sloping terrain. In fact, the southwest vortex, influenced by steep topography associated with the Tibetan Plateau, accounts for the bulk of the convective rainfall, sometimes at extremely high rates, in the SBM region (Kuo et al. 1988; Fu et al. 2014). A 14-yr southwest vortex climatology reveals that about 72% of such systems are accompanied with thunderstorms (Fu et al. 2014). Some long-lived vortex systems could influence rainfall production along the middle and lower reaches of YRB, after moving out of the Sichuan basin (e.g., Li et al. 2014).

Figure 4a also shows that high-density centers exceeding 4 flashes $km^{-2}\,yr^{-1}$ are distributed roughly along the Yangtze and Huaihe Rivers. The Yangtze River delta is an active flash region with several high-flash-density areas. Their generations do not seem to be attributable directly to any sloping topography.

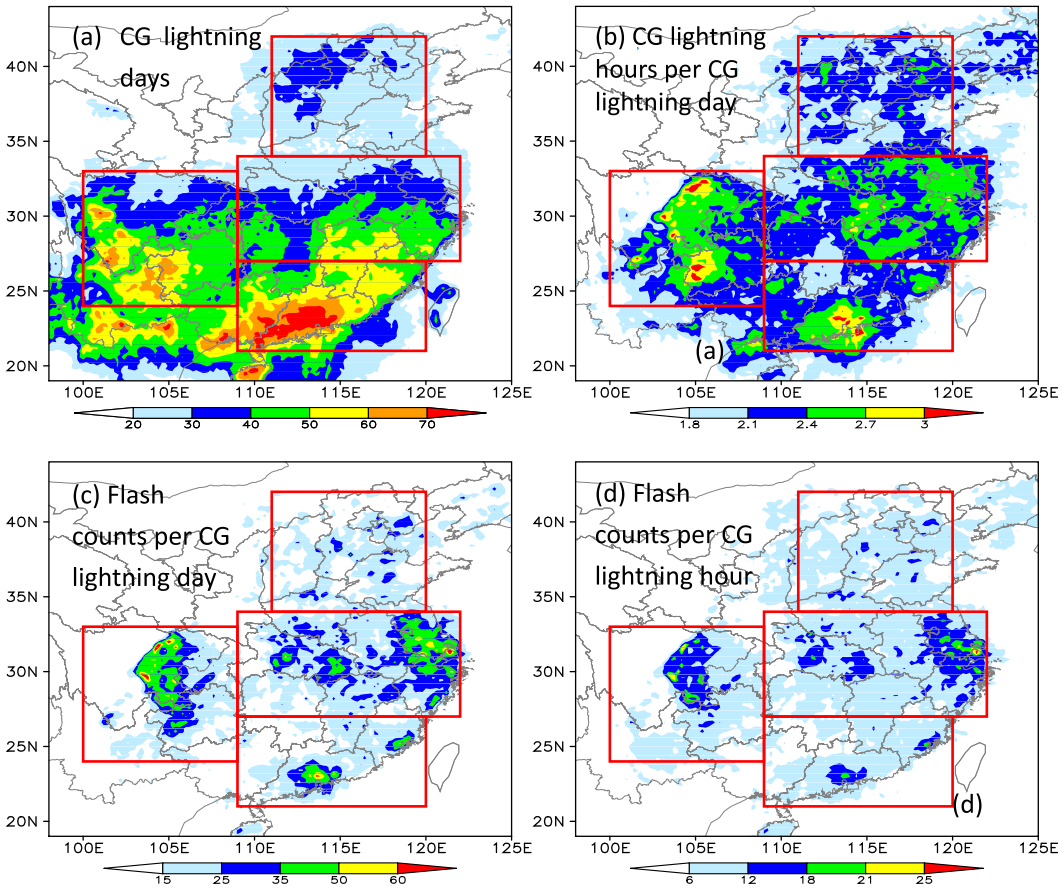

FIG. 5. Spatial distribution of (a) the number of CG lightning days (a CG lightning day is recorded when a CG lightning flash occurred during one day between 0000 and 2300 Beijing standard time) per year, (b) the number of CG lightning hours (a CG lightning hour is recorded when a CG lightning flash occurred during 1 h) per CG lightning day, (c) flash counts per CG lightning day, and (d) flash counts per CG lightning hour at 0.2° × 0.2° grid resolution for the 6-yr period of 2008–13 over central and eastern China.

However, this region is dominated by warm and moist monsoon air during summer, and experiences the passages of mesoscale convective systems (MCSs), such as those associated with the southwest vortex, tropical storms, and those propagating along quasi-stationary mei-yu fronts that may extend from YRB to Korea and Japan (Tao 1980; Ding and Chan 2005). The interaction of sea–land-breeze circulation patterns with local topography may also contribute to the generation of several flash-density centers along the eastern coast of China.

Since positive flashes are often considered to be a measure of severity for convective storms (e.g., those producing hailstones or high winds), their spatial distribution for the study period is plotted in Fig. 4b, showing that most positive-flash-density centers exceeding 0.2 flashes $km^{-2} yr^{-1}$ coincide with the flash-density centers exceeding 3 flashes $km^{-2} yr^{-1}$. The Yangtze River estuary has the lowest proportion of positive flashes. In contrast, NC has higher percentages of positive flashes in spite of its lower flash density. Relatively high positive flash activity also appears on the eastern slope of Mount Daba and the northern slope of Mount Wuyi.

It is evident from the above analysis that the selected four target areas may be regarded as being representative for studying the CG lightning climatology in China, since they include almost all the major regions of CG lightning activity.

c. *Spatial distribution of annual CG lightning days and hours*

Figure 5a shows the spatial distribution of annual CG lightning days, whose values range from less than 30 days yr^{-1} over most of the NC region to more than 70 days yr^{-1} in the CG lightning maxima in the Pearl River delta. Because a CG lightning day is recorded regardless of the occurrence of one or multiple CG lightning flashes, unless

the CG lightning-producing MCS moved through a grid cell across daily boundaries (i.e., at 0000 LST), the recorded spatial coverage represents reasonably well the footprint of the MCS. Thus, the spatial patterns of annual CG lightning days look much smoother than those of the annual CG lightning flash density (cf. Figs. 5a and 4a), with the magnitudes decreasing smoothly from SBM eastward, and from SC northeastward to YRB and NC. The northeastward decrease in the CG lightning days appears to reflect well the northward progression of monsoon rainfall (Ding and Chan 2005). It is interesting that more distinct CG lightning days (than those over the surrounding regions) occur in mountainous regions, for example, in the northwestern portion of NC and in the western portion of SBM, where the CG lightning flash counts per CG lightning day are low (cf. Figs. 5a and 5c). This may be attributable to the frequent topographical triggering of thunderstorms but with short-lived life spans, which can be seen by comparing Figs. 5b and 5a.

Unlike the annual CG lightning flash density, few localized features in the annual CG lightning days appear in YRB and the Sichuan basin. In fact, the CG lightning days associated with the localized high CG lightning flash-density centers over the two regions are much less than those over mountainous regions where the CG lightning flash density is low. This can been seen by comparing Figs. 5b and 4a, where the high-density centers coincide with longer CG lightning hours, implying longer-lived thunderstorms; the opposite is true for low CG lightning flash-density locations. This can be further seen by comparing Figs. 5c and 5d, as these thunderstorms tend to produce high-frequency CG lightning flashes (e.g., as high as 60 flashes per CG lightning day or 25 flashes per CG lightning hour, especially in the Yangtze River delta region). It is interesting that the general coverage and the peak magnitude of both the flash counts per CG lightning day and per CG lightning hour over the Sichuan basin and the Yangtze River delta region are even greater than those in the CG lightning flash maxima in the Pearl River delta. This appears to indicate different dynamical and cloud microphysical processes associated with the CG lightning production over these regions. Clearly, this could be an interesting subject for future studies.

Figures 5c and 5d also show high flash counts per CG lightning day and also per CG lightning hour to the east of the mountainous regions in NC and the Sichuan basin. When integrating these results with the high CG lightning days per year and the high CG lightning hours per CG lightning day, given in Figs. 5a,b, we may assume that most thunderstorms accounting for the high flash counts are triggered over the mountainous regions and then moved eastward into the plain areas. Some of the thunderstorms may be nocturnal when they are formed during afternoon hours (He and Zhang 2010; Qian et al. 2015).

d. Spatial distribution of seasonal CG lightning flash density

Figure 6 shows the spatial distribution of the seasonal flash density over the four target regions. Marked differences in magnitude and pattern occur from region to region during all four seasons. In the spring, active CG lightning occurs only in south China (Fig. 6a; i.e., to the south of 30°N), with three distinct areas (i.e., in the Pearl River delta, over the Yunnan–Guizhou Plateau and Mount Wuyi). After entering the summer season, high CG lightning activity expands northward to north and northeast China (Fig. 6b). More significantly, the locations of major flash-density centers in SBM and YRB are shifted from the Yunnan–Guizhou Plateau and Mount Wuyi to the Sichuan basin and the lower reach of YRB, respectively. These shifts occur after the onset of the South China Sea summer monsoon and the development of a quasi-stationary meiyu front in June, which formed along the YRB because of the meeting of northwesterly colder air with warm and moist monsoonal air from the south, during the warm season (Ding and Chan 2005). The seasonal flash-density structures, including the three major flash density centers, are similar to the corresponding annual structures (cf. Figs. 6b and 4a). On average, the summer flash density more than doubles in magnitude that in the spring, especially at the three major centers. The results indicate that the summer CG lightning occurrences account for a large percentage of the annual total flash counts. After all, the moisture supply in the southwesterly monsoonal air is the most abundant for organized MCSs in the summer over central and eastern China (Zheng et al. 2008).

In autumn, CG lightning activity retreats southward to southeastern (and southern) China, as expected, with much reduced intensities everywhere (Fig. 6c). Note the presence of a west–east-oriented CG lightning zone, albeit with a small density of 0.1–0.5 flashes $km^{-2} yr^{-1}$, in the northern portion of NC that is in distinct contrast with the little CG lightning activity to the south. CG lightning activity almost disappears in NC, SBM, and even in SC during winter (Fig. 6d). This could be clearly attributed to the presence of the weakest solar heating and the least available water content in the low troposphere during the cold season. However, YRB could still experience CG lightning activity, although its intensity is extremely small. Its peak value is about 0.18 flashes $km^{-2} yr^{-1}$, which is less than 8% and 3% of that in autumn and summer, respectively. The associated convective conditions, though very weak, could not be attributed to the surface heating but to some middle- and upper-level processes, for example, vertical differential thermal

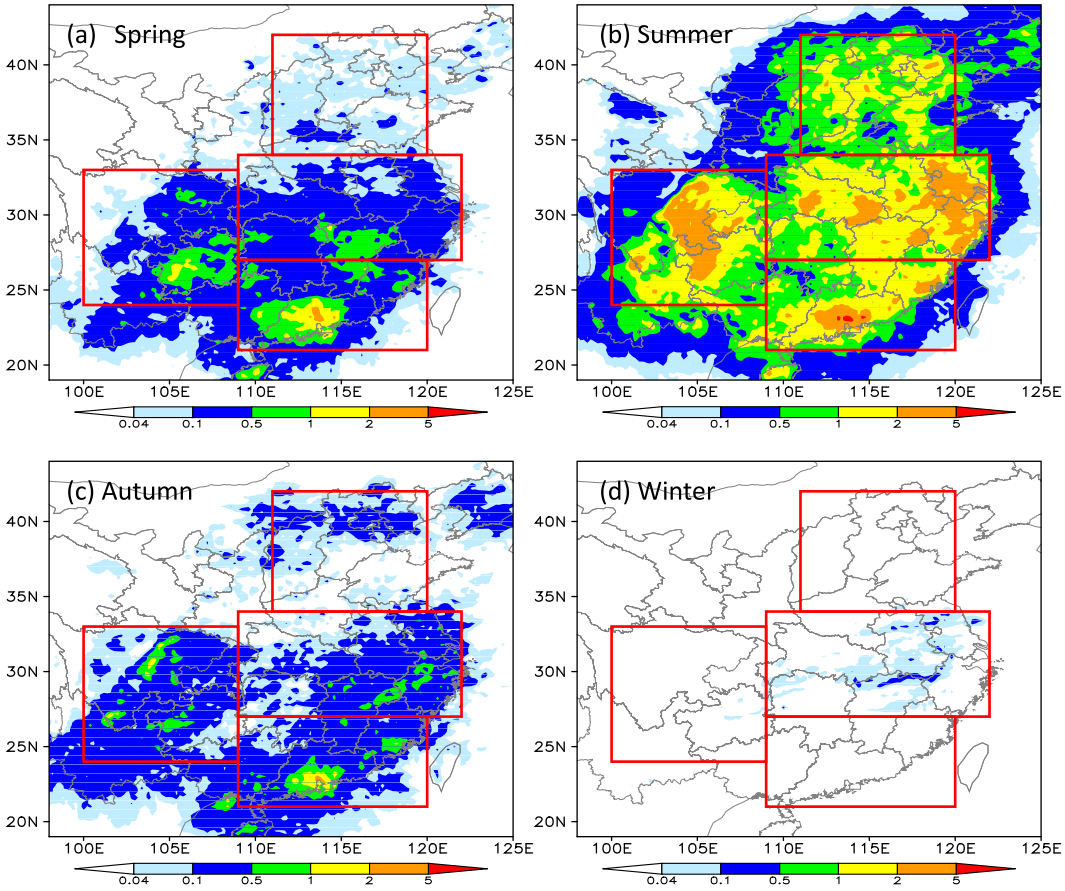

FIG. 6. Spatial distribution of the seasonal CG lightning density (shaded, flashes $km^{-2}\,yr^{-1}$) for (a) spring (March–May), (b) summer (June–August), (c) autumn (September–November), and (d) winter (December–February) at $0.2° \times 0.2°$ grid resolution for the 6-yr period of 2008–13 over central and eastern China.

advection with cold polar air over the underlying warmer and moisture air (Zhou 2011).

e. *Monthly variation of CG lightning flash density*

Figure 7 shows the monthly distribution of the area-averaged flash density over the four regions. Like those shown in Fig. 6, the warm (cold) season exhibits the highest (lowest) CG lightning activity, with the peak (smallest) amplitudes occurring in August (December and January), which agrees with the annual cycle of CG lightning over the other areas of the Northern Hemisphere. Note the near-linear growth in flash density from February to August, but sharp decreases subsequently, with nearly negligible amounts in October, except for in SC. Of interest is that YRB has the highest mean flash density of 0.54–0.72 flashes $km^{-2}\,month^{-1}$ during July and August, which is even higher than that of SC; the same is also true for March and November. The former scenario could be attributed to the wide coverage of moderate-to-high CG lightning activity (cf. Figs. 7 and 6b) associated with extensive rainfall along quasi-stationary mei-yu fronts. Similarly, the mean CG lightning activity in SBM is close to that in SC during July and August.

By comparison, the proportions of positive flashes are typically lowest in July and August, but highest during the months of December–February, except for NC whose peak value occurs in April. For example, in SC, this proportion is about 3% in summer but as high as 68% in winter. This proportion increases slightly and decreases significantly northward in the warm and cold seasons, respectively. This indicates that most flashes are generated in MCSs with different cloud microphysics processes or under different larger-scale meteorological conditions. The above phenomena of the respective high and low proportionalities in winter and summer are in qualitative agreement with previous works (Orville and Huffines 2001; Bentley and Stallins 2005; Rivas Soriano et al. 2005; Antonescu and Burcea 2010). But the average percentage of positive flashes in winter from these studies was about 25%, which is smaller

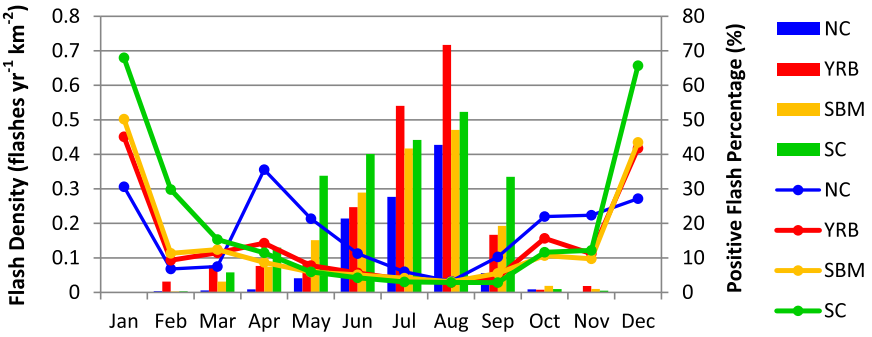

FIG. 7. Monthly variation of the regional mean CG lightning density (colored bars; flashes $km^{-2}\,yr^{-1}$) and the regional mean percentage of positive CG lightning density (colored lines) for the four target regions given in Fig. 1 for the 6-yr period of 2008–13.

than that reported herein, although high percentages of 52%–59% had been observed in some winter precipitation cases in the United States (e.g., Holle and Watson 1996). High proportions of positive flashes have also been observed in the other eastern Asian regions. Brook et al. (1982) noted that about 41% of the CG lightning strokes in eight winter storms along the Hokuriku coast of Japan were positive. Eom and Suh (2009) examined the CG lightning climatology in Korea during 2002–06 and found about 50% of positive CG lightning flashes occurred during the month of February.

f. Diurnal cycle of CG lightning activity

As we know, CG lightning could occur at any time of day during rainy seasons. Thus, it is of more interest to know the typical hours of a day at which CG lightning peaks. For this reason, Figs. 8a,b show spatial distributions of the peak CG lightning hours over central and eastern China during the warm and cold seasons, respectively, as two extreme scenarios. It is evident that the YRB and SC regions are dominated by late-afternoon peak CG lightning hours (i.e., 1500–1800 LST) during the warm season (Fig. 8a), except for a few isolated locations where the peak CG lightning activity is delayed for 2–3 h. Of relevance is that less CG lightning activity takes place during the evening hours despite the frequent generation of nocturnal heavy rainfall over these regions (Liu et al. 2008), indicating that a significant portion of nocturnal heavy rainfall may be stratiform in nature and produced by warm cloud microphysical processes.

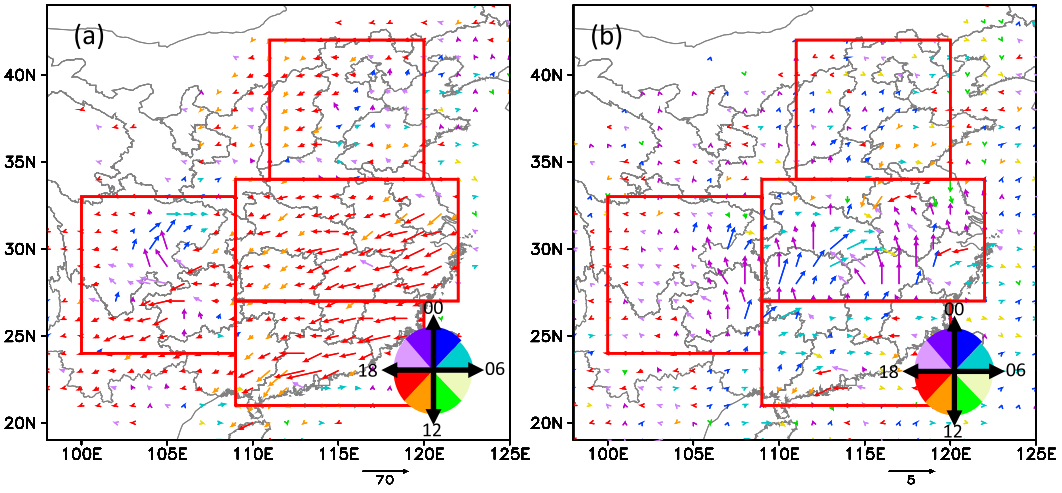

FIG. 8. Spatial distribution of the peak CG lightning hour and the hourly averaged CG lightning counts at the peak hour (flashes) during the (a) warm season (May–September) and (b) cold season (November–March) at 1° × 1° grid resolution for the 6-yr period of 2008–13 over central and eastern China. The vector length denotes the hourly averaged CG lightning counts at the peak CG lightning hour (LST), which is shown by the vector direction in the right-bottom corner. The vector pointing north (south, east, west) indicates the time of midnight (1200, 0600, and 1800 LST), and the following 3 h share one color. Note the different vector length scales used for the two panels.

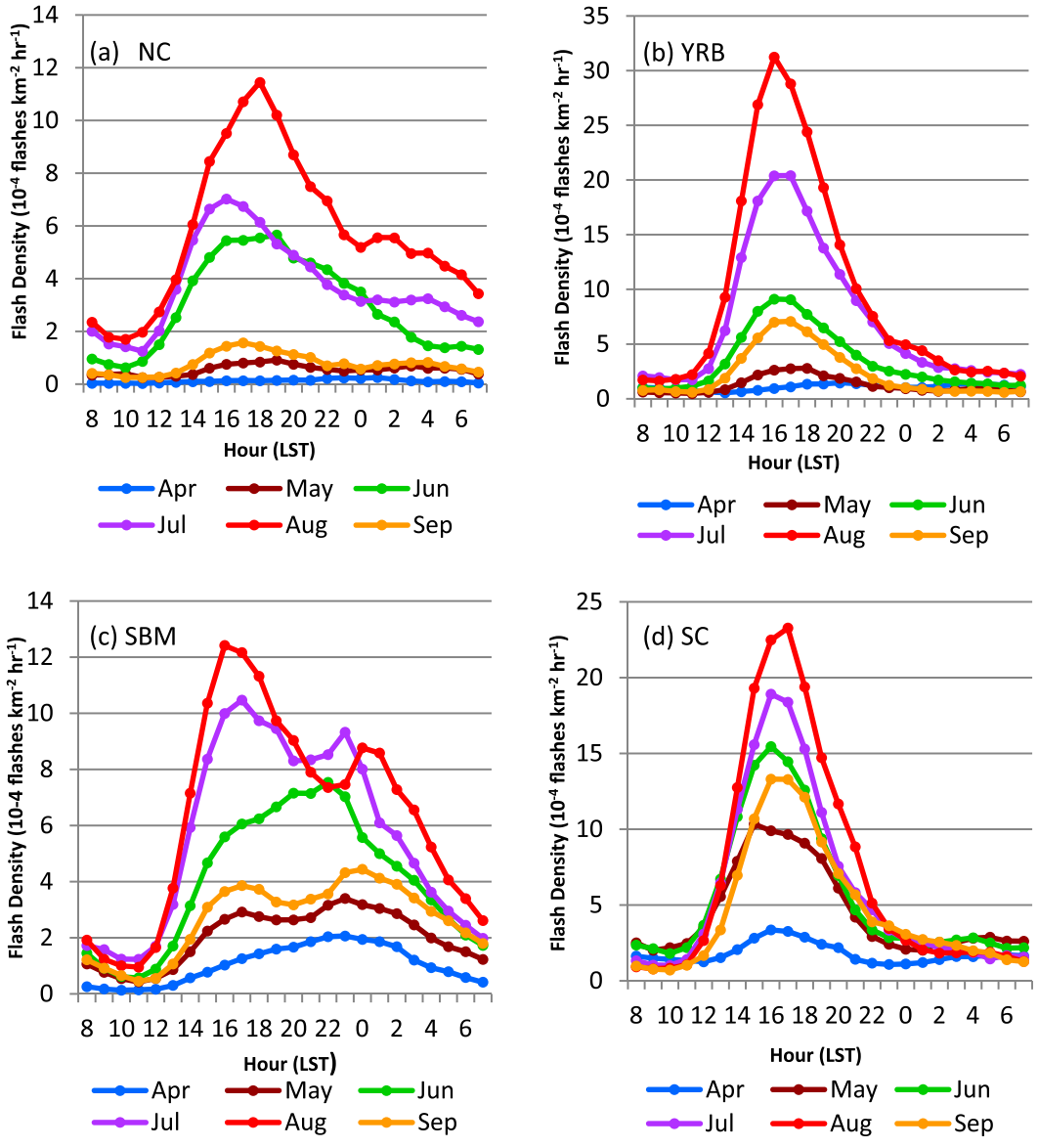

FIG. 9. Diurnal variation of the hourly CG lightning density (10^{-4} flashes km^{-2} h^{-1}) during the months of April–September for (a) NC, (b) YRB, (c) SBM, and (d) SC for the 6-yr period of 2008–13. Note the different vertical scales used for different regions.

Of particular interest is that while the late afternoon peak CG lightning hours also take place over mountainous areas in NC and SBM, their downstream plain or basin areas exhibit peak CG lightning activity from the evening to early morning hours. This result is consistent with the presence of more (fewer) CG lightning days over the high-elevation (downstream plain or basin) areas (cf. Figs. 8a and 5a), indicating further that more deep convection is triggered over the mountainous areas during the afternoon hours, and then displaced to the downstream plain or basin areas.

Note that the peak-hour distribution in the cold season differs markedly from that in the warm season (Fig. 8b). On the one hand, the afternoon peak CG lightning hours are no longer evident in most parts of the four regions, indicating that solar heating could not explain the development of CG lightning activity in winter. On the other hand, little topographical impact on the CG lightning production could be seen in high-elevation areas. Instead, more active CG lightning in YRB and the eastern portion of SBM appears around midnight and in the early morning hours. Most parts of SC also have early morning peak hours for CG lightning.

Figures 9a–d show the diurnal cycles of the regional mean flash density during the months of April–September

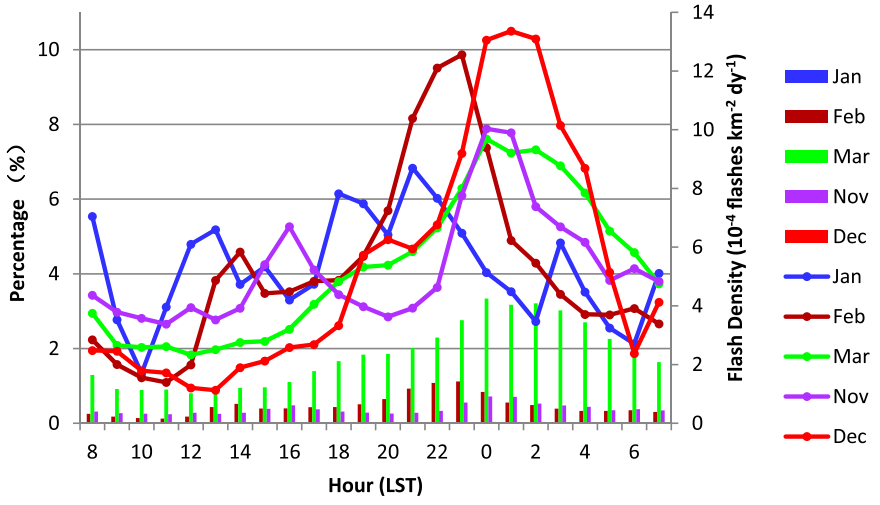

FIG. 10. The diurnal variation of the percentage (colored lines) of the hourly CG lightning density (10^{-4} flashes $km^{-2}\,h^{-1}$) with respect to the daily total CG lightning density (10^{-4} flashes $km^{-2}\,h^{-1}$; colored bars) during the months of November–March for all the four target regions during the 6-yr period of 2008–13.

over the four regions. We can see from Figs. 9b and 9d that the diurnal CG lightning cycle over YRB resembles closely that over SC, only differing in their peak magnitudes. That is, the hourly flash density grows rapidly after noontime and reaches its peak at 1600 or 1700 LST. Then, it decreases sharply until 2200–2300 LST, after which time much less CG lightning activity continues for the rest of evening hours. The daily peak flash counts in YRB increase markedly from June to July and August, and then drop sharply in September, whereas those in SC increase markedly from April to May, and evolve relatively slowly during the subsequent months. Moreover, a single-peak diurnal cycle dominates the warm months, except for a secondary early evening peak during the months of April and May over SC.

In contrast, both the SBM and NC regions show double peaks in flash counts, with one in the late afternoon and the other during the evening hours (Figs. 9a,c). Unlike in the other three regions, the late-afternoon peak over SBM is only secondary, with the primary peak occurring just prior to midnight, in the months of April–June (Fig. 9c). Furthermore, the secondary flash-density peak near midnight during the months of July and August is more distinct than that in the other three regions. This appears to be attributable to the development of thunderstorms triggered by downslope winds from the western Sichuan Plateau, as well as rainfall systems moving northeastward downslope of the Yunnan–Guizhou Plateau toward the Sichuan basin from the late evening to the early morning (Yu et al. 2009; Qian et al. 2015). The secondary CG lightning peak in NC appears after midnight during the warm season, except for the month of June, during which little evidence of double CG lightning peaks is present (Fig. 9a).

The diurnal variations of the hourly CG lightning flash percentages during the cold season for the four regions are given in Fig. 10, showing slow growth in CG lightning activity from the morning to afternoon hours, with more fluctuations in the month of January resulting likely from the existence of fewer samples, as shown by the short color bars. Although the CG lightning activity tends to have a secondary peak during the afternoon hours, its primary peak occurs around midnight, and then decreases quickly afterward. The least CG lightning activity occurs between 1000 and 1200 LST, which is similar to that during the warm season (cf. Figs. 9 and 10).

In summary, the peak hourly flash counts near midnight suggest the presence of some large-scale destabilizing processes (e.g., differential thermal or moisture advection) during the cold season, whereas the hourly flash counts reach their maximum values in the afternoon hours during the warm season revealing that most flashes are generated by deep convection associated with the surface heating, which may be aided by topographical forcing.

4. Relationship between CG lightning activity and rainfall

Because precipitation and lightning are closely associated with convective processes, considerable research has been conducted during the past decade to examine to what extent the two variables are correlated (e.g., Kempf and Krider 2003; Pessi and Businger 2009; Xu et al. 2013;

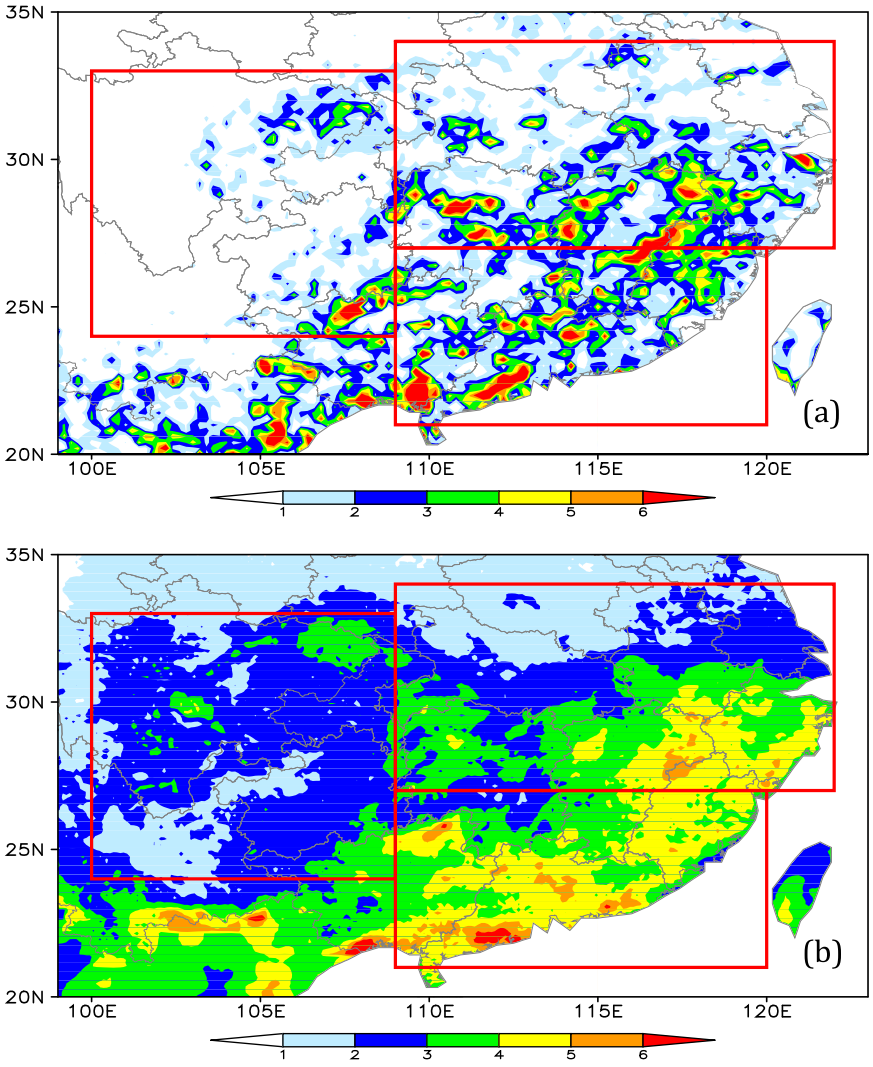

FIG. 11. Comparison of daily average rainfall rates (mm day^{-1}) derived by (a) TRMM PR to that of (b) 0.1°-resolution hourly rain gauge data during the 6-yr period of 2008–13. Values in (a) are obtained, following Fu et al. (2008), as ratios of the summed rainfall from detected pixels to the total numbers of pixels, which are then multiplied by 24 h.

Stolz et al. 2014). Moreover, numerous studies have estimated the rain yield value, defined as the rain mass per CG lightning flash, to determine the location and intensity of convective rainfall and to help assimilate lightning data in numerical weather prediction models (e.g., Petersen and Rutledge 1998; Gungle and Krider 2006). Although the previous studies revealed close correlation between precipitation and lightning, the relationship between them is highly nonlinear and complicated such that heavy rainfall events may contain little lightning activity and vice versa. Xu et al. (2013) showed that only 50% of total lightning flashes could be correlated to heavy rainfall regions in an MCS. Although searching for such a correlation is beyond the scope of the present study, it is desirable to see how the CG lightning climatology shown in section 3 is related to its corresponding rainfall climatology.

Since lightning occurs rarely in stratiform regions, we separate the convective and stratiform rainfall during the study period using the TRMM PR 2A25 products. Because the TRMM PR's detected range was within 38°N, we focus only on the analysis of rainfall occurring over SC, SBM, and YRB. As a first step, Fig. 11 compares the daily average rainfall derived by TRMM PR measurements to that analyzed by 0.1°-resolution hourly rain gauge data to ensure the statistical significance of using 6-yr TRMM PR 2A25 products. Results show similar rainfall patterns from the two different

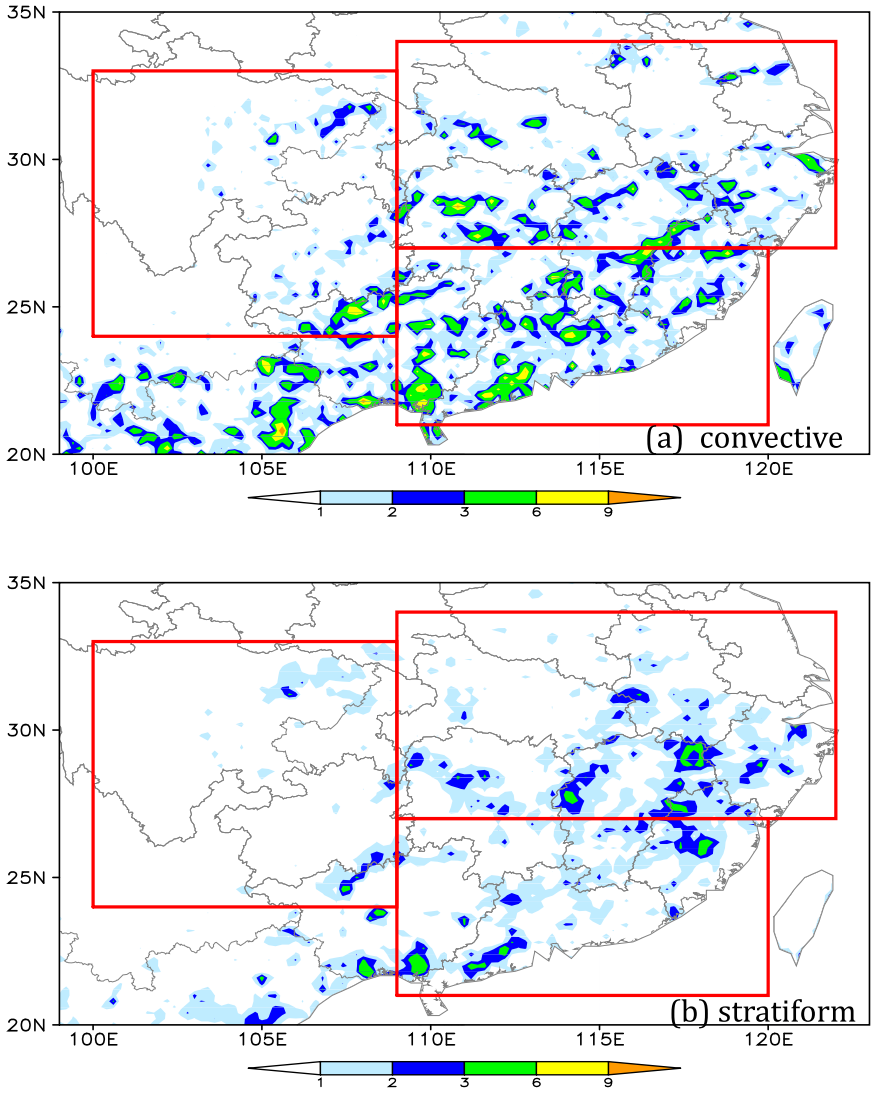

FIG. 12. Daily averaged (a) convective and (b) stratiform rainfall rates (mm day^{-1}) observed by TRMM PR during the 6-yr period of 2008–13.

data sources, although some differences are also apparent. Both datasets exhibit a major rainfall belt distributed along the coastal regions (i.e., within a 600-km distance inland from the coastline from southern China to the Yangtze River delta), where the warm and moist air of the southwesterly monsoon typically prevails during the warm season. Rainfall centers in Guangdong, Fujian, and YRB are also comparable between the two datasets.

Given the reasonable total rainfall structures of the TRMM PR data, we may examine to what extent CG lightning flash density and days are correlated to convective rainfall in TRMM PR. We see that the general patterns of convective rainfall along the coastal regions are similar to those of CG lightning flash density and days (cf. Figs. 12a, 4a, and 5). However, high-flash-density centers are not highly correlated to large rainfall centers. For example, the CG lightning flash maxima does not coincide with the heavy rainfall center in Guangdong. Moreover, the high-flash-density regions in SBM correspond to small daily average rainfall regions, whereas the large rainfall regions to the south of SBM do not produce high flash densities. It follows that although there might be correlations between the annual CG lightning and rainfall climatology at the regional scales, such correlations at some locations do not always seem to be evident.

The monthly variations of the regional convective, stratiform, and total rainfall over YRB, SBM, and SC are given in Fig. 13, showing that both the convective rainfall and total rainfall are peaked in May for SC, which

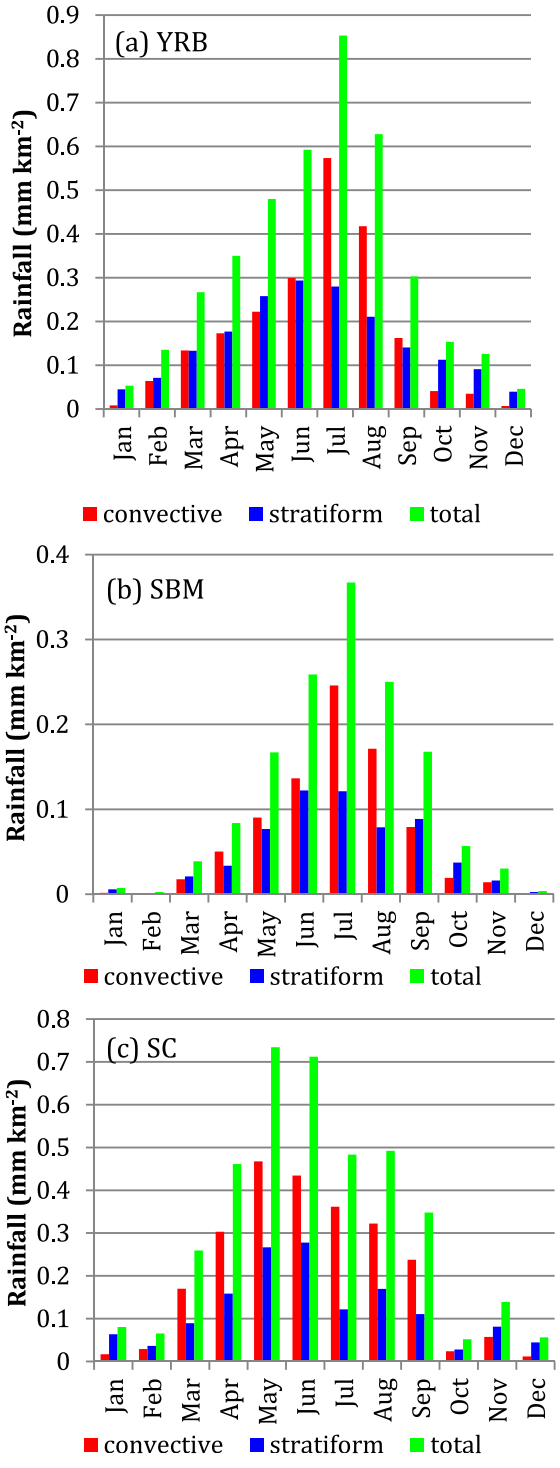

FIG. 13. Monthly variation of the regional convective, stratiform, and total rainfall (colored columns; mm km^{-2}) for (a) YRB, (b) SBM, and (c) SC observed by TRMM PR during the 6-yr period of 2008–13.

coincide with the onset of summer monsoon, and in July for YRB and SBM, which correspond to the establishment of the mei-yu frontal rainfall systems. Obviously, the peak rainfall months in the three regions differ from the peak CG lightning month of August for all the regions (cf. Figs. 13 and 7). Furthermore, stratiform rainfall presents different peaks from convective rainfall (i.e., in June when the monsoonal rainfall becomes predominant). The convective rainfall is almost twice the stratiform rainfall for the three regions during late summer, and this phenomenon lasts from March to September in SC.

Figure 14 shows the diurnal cycles of convective, stratiform, and total rainfall during the warm season. Note first that the 3-hourly total rainfall tendencies from TRMM PR are similar to those obtained from the hourly rain gauge data (not shown). Like the CG lightning flash density, the diurnal cycles of the regional convective rainfall in SC and YRB are similar to each other (Figs. 14a,c), that is, exhibiting double rainfall peaks: one in the afternoon and the other during the late night to morning, with a minimum at midnight. Stratiform rainfall over YRB increases during the late night to early morning, leading to a distinct peak in total rainfall in the early morning hours, as compared to the other regions. This result supports our earlier conjecture that a significant portion of nocturnal heavy rainfall with much less lightning activity in YRB is stratiform in nature, as shown in Figs. 8a and 9b. Similarly, stratiform rainfall becomes equally important as its convective counterpart during the early morning hours over SBM. By comparison, stratiform rainfall in SC fluctuates during the daytime, with few diurnal variations and less production than convective rainfall at all times. This is consistent with the presence of typically deep moist columns in the vast monsoonal airstreams during the warm season.

As compared with the regional diurnal cycles over YRB and SC, SBM exhibits quite different diurnal convective rainfall characteristics (Fig. 14b). That is, both the convective and stratiform rainfall amounts peak during the late-night hours (i.e., 0300–0500 LST), with minimum values during 1800–2000 LST. This implies more active CG lightning production but less rainfall production associated with afternoon convection.

5. Summary and conclusions

In this study, we have examined the spatial and temporal variations of CG lightning and rainfall during a 6-yr period from 2008 to 2013 over four active regions (i.e., NC, SC, YRB, and SBM) in central and eastern China. Results show the highest (lowest) flash counts in summer (winter) with the lowest (highest) proportion of positive flashes, especially in August (December and

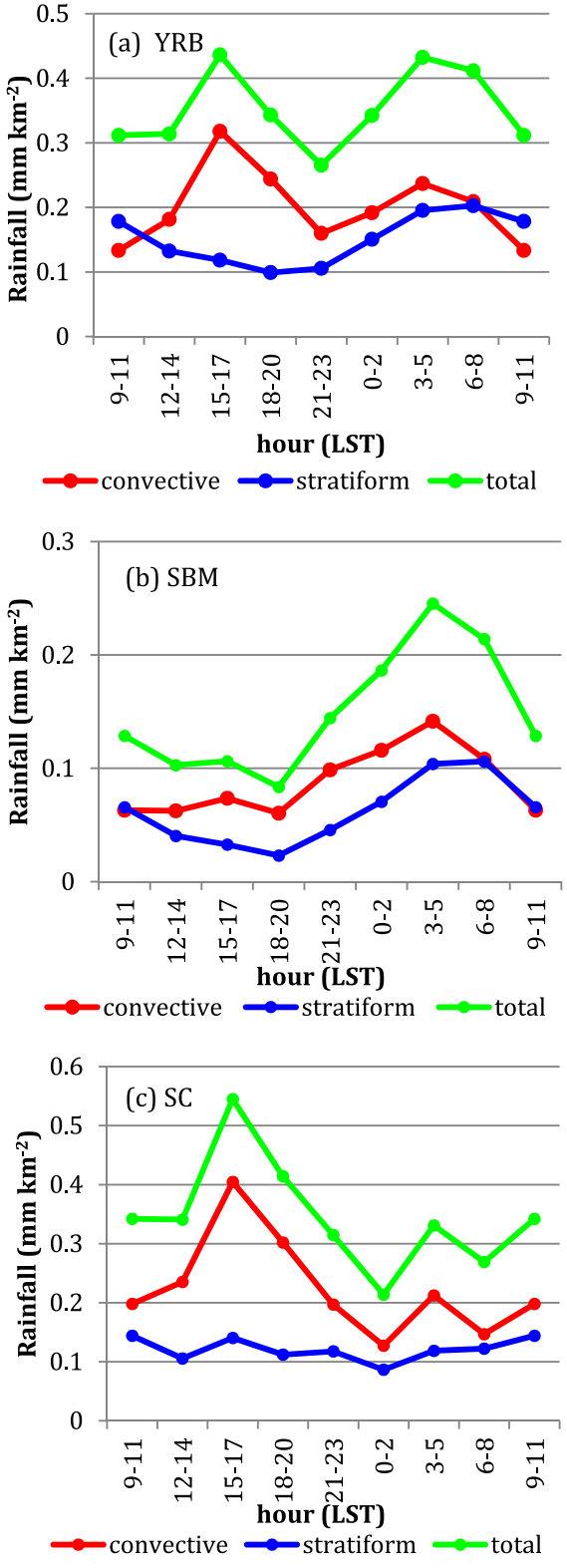

FIG. 14. Diurnal variation of 3-hourly convective, stratiform, and total rainfall (mm km^{-2}) during the warm season (May–September) for (a) YRB, (b) SBM, and (c) SC observed by TRMM PR during the 6-yr period of 2008–13.

January). Marked spatial variations of CG lightning are found, with some high-flash-density centers taking place at certain preferred locations. The highest flash densities, exceeding 9 flashes km^{-2} yr^{-1} and more than 70 CG lightning days yr^{-1}, are found in the northern Pearl River delta region, and they are generated mostly in spring, summer, and autumn. Following this concentrated CG lightning area are the Sichuan basin, the Yangtze River delta region, and the southeastern coastal region in that order. Results also show that NC is more CG lightning active in summer, whereas YRB could be CG lightning active in all seasons, albeit with large differences in magnitude.

A comparison of the convective rainfall climatology indicates similar patterns along the coastal regions. However, high-flash-density centers are not correlated to large rainfall centers. It is found that monthly convective rainfall is peaked in May or July, but the highest flash density appears in August. An analysis of the diurnal cycles shows a dominant CG lightning peak in the late-afternoon hours for all the regions, with a secondary CG lightning peak near midnight during the warm season for SBM and NC, but with double convective rainfall peaks: a higher one in the afternoon and the other from the late night to morning hours over SC and YRB. The SBM is dominated by a rainfall peak from late night to early morning. An analysis of the convective and stratiform rainfall from the TRMM PR data indicates that the proportion of stratiform rainfall over YRB and SBM increases from the late night to early morning hours, and equals closely that of convective rainfall with a distinct peak during the early morning hours. This nocturnal rainfall tendency is opposite to that of lightning activity. Taken together, these results suggest the important roles of surface heating and local topography in triggering deep convection and the different roles of short- versus long-lived MCSs and stratiform rainfall in determining the diurnal cycles of CG lightning and rainfall. In general, higher-frequency thunderstorm but lower-flash-density days occur over mountainous regions because of the development of short-lived afternoon storms, whereas higher-flash-density days, typically associated with nocturnal thunderstorms, appear over the north China plain and Sichuan basin. During the monsoon season fewer flashes are generated over the plain and basin areas in the late night to morning hours when hourly rainfall peaks.

In conclusion, we may state that substantial spatial and temporal variations in CG lightning climatology occur in central and eastern China and that these changes depend on latitude, season, month, the time of a day, local topography, and prevailing convective systems as well as larger-scale moisture and flow conditions. Some of the

variations are consistent with those of rainfall, whereas the others are not highly correlated. The results have important implications for the assimilation and parameterization of CG lightning for numerical weather prediction models. Of course, more work is needed to study regional CG lightning climatology, namely, high versus low flash density, in relation to the corresponding rainfall counterpart. In addition, rain yield values may be estimated to help understand the relationship between CG lightning and rainfall at various spatial and temporal scales.

Acknowledgments. We are grateful to Prof. Yunfei Fu of the University of Science and Technology of China and Prof. Yijun Zhang and Dr. Jinfang Yin of the Chinese Academy of Meteorological Sciences for their helpful discussions on data processing and to Mr. Qingtao Meng of CMA/National Meteorological Center for his assistance in accessing the CG lightning data. Constructive comments from three anonymous reviewers that resulted in significant improvements of the manuscript are also appreciated. This work was jointly supported by the National Basic Research Program of China (973 Program: 2014CB441402), the National Department Public Benefit Research Foundation (Grant GYHY201406003), and the National Natural Science Foundation of China (Grant 41205028).

REFERENCES

Antonescu, B., and S. Burcea, 2010: A cloud-to-ground lightning climatology for Romania. *Mon. Wea. Rev.*, **138**, 579–591, doi:10.1175/2009MWR2975.1.

Bentley, M. L., and J. Stallins, 2005: Climatology of cloud-to-ground lightning in Georgia, USA, 1992–2003. *Int. J. Climatol.*, **25**, 1979–1996, doi:10.1002/joc.1227.

Brook, M., M. Nakano, P. Krehbiel, and T. Takeuti, 1982: The electrical structure of the Hokuriku winter thunderstorms. *J. Geophys. Res.*, **87**, 1207–1215, doi:10.1029/JC087iC02p01207.

Changnon, S. A., Jr., 1964: Climatology of damaging lightning in Illinois. *Mon. Wea. Rev.*, **92**, 115–120, doi:10.1175/1520-0493(1964)092<0115:CODLII>2.3.CO;2.

Chronis, T., K. Cummins, R. Said, W. Koshak, E. McCaul, E. R. Williams, G. T. Stano, and M. Grant, 2015: Climatological diurnal variation of negative CG lightning peak current over the continental United States. *J. Geophys. Res. Atmos.*, **120**, 582–589, doi:10.1002/2014JD022547.

CMA, 2009: *China Lightning Monitoring Reports (2008)* (in Chinese). China Meteorological Press, 142 pp.

——, 2010: *China Lightning Monitoring Reports (2009)* (in Chinese). China Meteorological Press, 119 pp.

——, 2011: *China Lightning Monitoring Reports (2010)* (in Chinese). China Meteorological Press, 138 pp.

——, 2013: *China Lightning Monitoring Reports (2011)* (in Chinese). China Meteorological Press, 124 pp.

Cummins, K. L., and M. J. Murphy, 2009: An overview of lightning locating systems: History, techniques, and data uses, with an in-depth look at the U.S. NLDN. *IEEE Trans. Electromagn. Compat.*, **51**, 499–518, doi:10.1109/TEMC.2009.2023450.

——, ——, E. A. Bardo, W. L. Hiscox, R. B. Pyle, and A. E. Pifer, 1998: A combined TOA/MDF technology upgrade of the US National Lightning Detection Network. *J. Geophys. Res.*, **103**, 9035–9044, doi:10.1029/98JD00153.

Curran, E. B., R. L. Holle, and R. E. López, 2000: Lightning casualties and damages in the United States from 1959 to 1994. *J. Climate*, **13**, 3448–3464, doi:10.1175/1520-0442(2000)013<3448:LCADIT>2.0.CO;2.

Ding, Y.-H., and J. C. L. Chan, 2005: The East Asian summer monsoon: An overview. *Meteor. Atmos. Phys.*, **89**, 117–142, doi:10.1007/s00703-005-0125-z.

Enno, S., 2011: A climatology of cloud-to-ground lightning over Estonia, 2005–2009. *Atmos. Res.*, **100**, 310–317, doi:10.1016/j.atmosres.2010.08.024.

Eom, H. S., and M. S. Suh, 2009: Statistical characteristics of recent lightning occurred over South Korea (in Korean). *J. Korean Earth Sci. Soc.*, **30**, 210–222, doi:10.5467/JKESS.2009.30.2.210.

Fosdick, E. K., and A. I. Watson, 1995: Cloud-to-ground lightning patterns in New Mexico during the summer. *Natl. Wea. Dig.*, **19** (4), 17–24. [Available online at http://www.nwas.org/digest/papers/1995/Vol19-Issue4-Jul1995/Pg17-Fosdick.pdf.]

Fu, S., J. Zhang, J. Sun, and X. Shen, 2014: A fourteen-year climatology of the southwest vortex in summer. *Atmos. Oceanic Sci. Lett.*, **7**, 510–514, doi:10.3878/AOSL20140047.

Fu, Y., A. Zhang, Y. Liu, Y. Zheng, Y. Hu, S. Feng, and A. Cao, 2008: Characteristics of seasonal scale convective and stratiform precipitation in Asia based on measurements by TRMM precipitation radar (in Chinese). *Acta Meteor. Sin.*, **66**, 730–746.

Gungle, B., and E. P. Krider, 2006: Cloud-to-ground lightning and surface rainfall in warm-season Florida thunderstorms. *J. Geophys. Res.*, **111**, D19203, doi:10.1029/2005JD006802.

He, H., and F. Zhang, 2010: Diurnal variations of warm-season precipitation over northern China. *Mon. Wea. Rev.*, **138**, 1017–1025, doi:10.1175/2010MWR3356.1.

Hidayat, S., and M. Ishii, 1998: Spatial and temporal distribution of lightning activity around Java. *J. Geophys. Res.*, **103**, 14 001–14 009, doi:10.1029/97JD01576.

Holle, R. L., and A. I. Watson, 1996: Lightning during two central U.S. winter precipitation events. *Wea. Forecasting*, **11**, 599–614, doi:10.1175/1520-0434(1996)011<0599:LDTCUW>2.0.CO;2.

Huffines, G. R., and R. E. Orville, 1999: Lightning ground flash density and thunderstorm duration in the continental United States: 1989–96. *J. Appl. Meteor.*, **38**, 1013–1019, doi:10.1175/1520-0450(1999)038<1013:LGFDAT>2.0.CO;2.

Kempf, N. M., and E. P. Krider, 2003: Cloud-to-ground lightning and surface rainfall during the great flood of 1993. *Mon. Wea. Rev.*, **131**, 1140–1149, doi:10.1175/1520-0493(2003)131<1140:CLASRD>2.0.CO;2.

Koshak, W. J., K. L. Cummins, D. E. Buechler, B. Vant-Hull, R. J. Blakeslee, E. R. Williams, and H. S. Peterson, 2015: Variability of CONUS lightning in 2003-12 and associated impacts. *J. Appl. Meteor. Climatol.*, **54**, 15–41, doi:10.1175/JAMC-D-14-0072.1.

Kuo, Y.-H., L. Cheng, and J. W. Bao, 1988: Numerical simulation of the 1981 Sichuan flood. Part I: Evolution of a mesoscale southwest vortex. *Mon. Wea. Rev.*, **116**, 2481–2504, doi:10.1175/1520-0493(1988)116<2481:NSOTSF>2.0.CO;2.

Li, J., J. Du, D.-L. Zhang, C. Cui, and Y. Liao, 2014: Ensemble-based analysis and sensitivity of mesoscale forecasts of a vortex over southwest China. *Quart. J. Roy. Meteor. Soc.*, **140**, 766–782, doi:10.1002/qj.2200.

Liu, H., D.-L. Zhang, and B. Wang, 2008: Daily to submonthly weather and climate characteristics of the summer 1998

extreme rainfall over the Yangtze River basin. *J. Geophys. Res.*, **113**, D22101, doi:10.1029/2008JD010072.

Livingston, E. S., J. W. Nielsen-Gammon, and R. E. Orville, 1996: A climatology, synoptic assessment, and thermodynamic evaluation for cloud-to-ground lightning in Georgia: A study for the 1996 summer Olympics. *Bull. Amer. Meteor. Soc.*, **77**, 1483–1495, doi:10.1175/1520-0477(1996)077<1483:ACSAAT>2.0.CO;2.

López, R. E., and R. L. Holle, 1986: Diurnal and spatial variability of lightning activity in northeastern Colorado and central Florida during the summer. *Mon. Wea. Rev.*, **114**, 1288–1312, doi:10.1175/1520-0493(1986)114<1288:DASVOL>2.0.CO;2.

——, ——, A. I. Watson, and J. Skindlov, 1997: Spatial and temporal distributions of lightning over Arizona from a power utility perspective. *J. Appl. Meteor.*, **36**, 825–831, doi:10.1175/1520-0450-36.6.825.

Ma, M., W. Lyu, Y. Zhang, Q. Meng, and J. Yang, 2008: Characteristics of lightning exposure in China from 1997 to 2006 (in Chinese). *J. Appl. Meteor. Sci.*, **19**, 393–400.

Murphy, M. J., and R. L. Holle, 2005: Where is the real cloud-to-ground lightning maximum in North America. *Wea. Forecasting*, **20**, 125–133, doi:10.1175/WAF844.1.

Novák, P., and H. Kyznarová, 2011: Climatology of lightning in the Czech Republic. *Atmos. Res.*, **100**, 318–333, doi:10.1016/j.atmosres.2010.08.022.

Orville, R. E., 2008: Development of the National Lightning Detection Network. *Bull. Amer. Meteor. Soc.*, **89**, 180–190, doi:10.1175/BAMS-89-2-180.

——, and A. C. Silver, 1997: Lighting ground flash density in the contiguous United States: 1992–95. *Mon. Wea. Rev.*, **125**, 631–638, doi:10.1175/1520-0493(1997)125<0631:LGFDIT>2.0.CO;2.

——, and G. R. Huffines, 2001: Cloud-to-ground lightning in the United States: NLDN results in the first decade, 1989–98. *Mon. Wea. Rev.*, **129**, 1179–1193, doi:10.1175/1520-0493(2001)129<1179:CTGLIT>2.0.CO;2.

——, ——, W. R. Burrows, R. L. Holle, and K. L. Cummins, 2002: The North American Lightning Detection Network (NALDN)—First results: 1998–2000. *Mon. Wea. Rev.*, **130**, 2098–2109, doi:10.1175/1520-0493(2002)130<2098:TNALDN>2.0.CO;2.

Pan, Y., Y. Shen, J. Yu, and P. Zhao, 2012: Analysis of the combined gauge-satellite hourly precipitation over China based on the OI technique. *Acta Meteor. Sin.*, **70**, 1381–1389.

Pessi, A., and S. Businger, 2009: Relationships among lightning, precipitation, and hydrometeor characteristics over the North Pacific Ocean. *J. Appl. Meteor. Climatol.*, **48**, 833–848, doi:10.1175/2008JAMC1817.1.

Petersen, W. A., and S. A. Rutledge, 1998: On the relationship between cloud-to-ground lightning and convective rainfall. *J. Geophys. Res.*, **103**, 14 025–14 040, doi:10.1029/97JD02064.

Qian, T., P. Zhao, F. Zhang, and X. Bao, 2015: Rainy-season precipitation over the Sichuan basin and adjacent regions in southwestern China. *Mon. Wea. Rev.*, **143**, 383–394, doi:10.1175/MWR-D-13-00158.1.

Rakov, V. A., and M. A. Uman, 1990: Some properties of negative cloud-to-ground lightning flashes versus stroke order. *J. Geophys. Res.*, **95**, 5447–5453, doi:10.1029/JD095iD05p05447.

Reap, R. M., and D. R. MacGorman, 1989: Cloud-to-ground lightning: Climatological characteristics and relationships to model fields, radar observations, and severe local storms. *Mon. Wea. Rev.*, **117**, 518–535, doi:10.1175/1520-0493(1989)117<0518:CTGLCC>2.0.CO;2.

Rivas Soriano, L., F. de Pablo, and C. Tomas, 2005: Ten-year study of cloud-to-ground lightning activity in the Iberian Peninsula. *J. Atmos. Solar-Terr. Phys.*, **67**, 1632–1639, doi:10.1016/j.jastp.2005.08.019.

Stolz, D. C., S. Businger, and A. Terpstra, 2014: Refining the relationship between lightning and convective rainfall over the ocean. *J. Geophys. Res. Atmos.*, **119**, 964–981, doi:10.1002/2012JD018819.

Tao, S., 1980: *Heavy Rainfalls in China* (in Chinese). Science Press, 225 pp.

Vogt, B. J., and S. J. Hodanish, 2014: A high-resolution lightning map of the state of Colorado. *Mon. Wea. Rev.*, **142**, 2353–2360, doi:10.1175/MWR-D-13-00334.1.

Wang, D., S. Zhong, Y. Liu, J. Li, K. Hu, S. Yang, C. Zhang, L. Sun, and Z. Gao, 2007: Advances in the study of rainstorm in Northeast China (in Chinese). *Adv. Earth Sci.*, **22**, 549–560.

Watson, A. I., R. E. López, and R. L. Holle, 1994: Diurnal cloud-to-ground lightning patterns in Arizona during the southwest monsoon. *Mon. Wea. Rev.*, **122**, 1716–1725, doi:10.1175/1520-0493(1994)122<1716:DCTGLP>2.0.CO;2.

Xie, P. P., and A. Y. Xiong, 2011: A conceptual model for constructing high-resolution gauge-satellite merged precipitation analyses. *J. Geophys. Res.*, **116**, D21106, doi:10.1029/2011JD016118.

Xu, W., R. F. Adler, and N.-Y. Wang, 2013: Improving geostationary satellite rainfall estimates using lightning observations: Underlying lightning–rainfall–cloud relationships. *J. Appl. Meteor. Climatol.*, **52**, 213–229, doi:10.1175/JAMC-D-12-040.1.

Yu, R., J. Li, and H. Chen, 2009: Diurnal variation of surface wind over central eastern China. *Climate Dyn.*, **33**, 1089–1097, doi:10.1007/s00382-008-0478-3.

Zhang, D.-L., and Coauthos, 2013: The Beijing extreme rainfall of 21 July 2012: ''Right results'' but for wrong reasons. *Geophys. Res. Lett.*, **40**, 1426–1431, doi:10.1002/grl.50304.

Zhang, W., Q. Meng, M. Ma, and Y. Zhang, 2011: Lightning casualties and damages in China from 1997 to 2009. *Nat. Hazards*, **57**, 465–476, doi:10.1007/s11069-010-9628-0.

Zheng, Y., J. Chen, and P. Zhu, 2008: Climatological distribution and diurnal variation of mesoscale convective systems over China and its vicinity during summer. *Chin. Sci. Bull.*, **53**, 1574–1586, doi:10.1007/s11434-008-0116-9.

Zhou, L., 2011: Impact of East Asian winter monsoon on rainfall over southeastern China and its dynamical process. *Int. J. Climatol.*, **31**, 677–686, doi:10.1002/joc.2101.